JOURNAL OF Materials CHEMISTRY

Modular assembly and phase study of two- and three-dimensional porous tin(IV) selenides

Homayoun Ahari,[a] Alan Lough,[a] Srebri Petrov,[a] Geoffrey A. Ozin*[a] and Robert L. Bedard[b]

[a]*Materials Chemistry Research Group, Lash Miller Chemical Laboratories, 80 St. George Street, University of Toronto, Toronto, Ontario, Canada, M5S 3H6*
[b]*UOP, 25 Algonquin Road, Des Plaines, Illinois, USA*

Received 2nd October 1998, Accepted 12th March 1999

The work presented focuses attention on a detailed powder and single crystal XRD structure analysis of materials that emerge successively in the hydrothermal synthesis of tetramethylammonium-templated porous tin(IV) selenides. Four phases have been identified in this system and three of them, orthorhombic and monoclinic polymorphs of two-dimensional porous layered $TMA_2Sn_3Se_7$ (TMA = tetramethylammonium) plus a novel tetragonal three-dimensional open-framework $TMA_2Sn_5Se_{10}O$ have been structurally characterized by single crystal XRD. The order of appearance and interconversion of these materials is shown to follow Oswald's law of successive reactions, which is further supported by Connolly surface calculations. In addition the thermal stability of the orthorhombic $TMA_2Sn_3Se_7$ phase is explored by *in situ* variable temperature PXRD under nitrogen and in vacuum, from which it is determined that the structural integrity of the framework is retained up to the point of template removal around 250 and 300 °C, respectively. The accumulated knowledge that has emerged from this study and earlier work allows a modular assembly pathway to be proposed that can rationalize the formation of the observed phases.

Introduction

Polymorphic materials are described as compounds, which have identical empirical formulae and usually different lattice type and space group. Since polymorphs share identical composition, their chemical properties tend to be similar however, their physical properties, which are strongly influenced by the arrangement of the constituent atoms in the unit cell, may be quite distinct. By varying the external conditions of a crystal, such as temperature and pressure, structural transitions can take place which are referred to as 'polymorphous transformations'.[1,2] These phase transitions have generally been categorized as: 'reconstructive' and 'displacive'.[1,2] While the former is governed by breaking and reforming of bonds (*e.g.*, graphite to diamond and quartz to cristobalite) the latter involves bond distortions. When compared to the reconstructive process, the structure changes that occur in displacive transitions are rather small (*e.g.* polymorphs of silica such as α- to β-quartz and α- to β-cristobalite).[1,2]

In thermodynamic terms, an equilibrium crystal structure is determined by the minimum Gibbs free energy. In the initial stages of a reaction several structural modifications of a material may form as unstable phases which are subsequently transformed into more stable ones. The 'Oswald-step-rule' which is also referred to as 'the law of successive reactions' states that in a reaction, the first phase to form is the least stable with its free energy lying closest to the initial state. Through successive reactions, several relatively stable phases may be produced such that the first phase is consumed and replaced with a thermodynamically more stable one.[3–5] Since a phase transition is a thermodynamic phenomenon, factors such as temperature and pressure prevailing at the time of crystallization greatly influence which structure predominates.[3,6]

Furthermore, several polymorphs can exist in equilibrium with one another if their free energy values are similar. However, only a single product would be observed if the energy barrier for interconversion between phases is high. It is possible however, for a phase to exist beyond its stability region if the rate of transformation between phases, under the prevailing conditions, is small. Such materials are referred to as 'metastable phases'. Examples include zeolites, diamond and several modifications of SiC which owing to the slow rate of transformation to their respective thermodynamically stable phase, only convert over a long period of time.[3,5,7] In the context of metastable phases and open-framework materials, the operation of the Oswald's rule is seen in the transformation from more to less open zeolite structures, a case in point being zeolite Y to zeolite A to sodalite and finally to quartz.[5,8]

Polytypism is considered to be a special case of polymorphism. It is defined as the condition where crystallized modifications of a substance have identical cell parameters in two dimensions while the value of the third parameter is dependent upon the stacking sequence of the crystal planes.[3,8–13] As a result of this kind of disorder and a corresponding increase in the entropy (S), polytypic materials are thermodynamically favored phases.[9–16]

Layered binary materials of the type MY_2 crystallize in a variety of polymorphic and polytypic modifications. Their layered structure provides them with additional flexibility and sensitivity to stacking faults enabling them to crystallize with a variety of layer sequences and space groups. Structures of layered solids such as CdI_2,[17] $CdBr_2$,[17] PbI_2,[17] SnS_2,[11–13] $SnSe_2$[18] and GeS_2[19] have been well studied. The various polytypes of SnS_2 and $SnSe_2$ crystallize in hexagonal and rhombohedral lattice systems.[18]

The existence of polymorphism in layered microporous tin sulfide materials has been established.[20–22] For these materials the nature of the organic template and water guest molecules found between and within the pores play a crucial role in determining the symmetry of the final products. In addition, the choice of synthesis conditions such as temperature and heating period can dramatically affect the structure of the product phase.[20–22] Furthermore, the unit cell of various members of the family of microporous metal sulfides undergoes reversible phase transformations as a result of the adsorption–desorption of physisorbed water. These observations demonstrate the unique flexibility of the structure and sensitivity of the layer organization to the type and concentration of guest molecules. This property engenders interest in the materials for chemical sensing.[23]

Here, we focus attention on a detailed powder and single crystal XRD structure analysis of materials emerging in the

hydrothermal synthesis profile of microporous tin(IV) selenides. Four phases have been identified and as a result of studying the time evolution of products in this system three have been structurally characterized. To amplify, the single crystal XRD structures of orthorhombic and monoclinic polymorphs of two-dimensional microporous layered $TMA_2Sn_3Se_7$ (TMA = tetramethylammonium) and a novel tetragonal three-dimensional open-framework $TMA_2Sn_5Se_{10}O$ are described. The order of appearance and interconversion of these materials is shown to follow the Oswald law of successive reactions. This may be the first time that the Oswald rule has been found to apply to non-oxide open-framework materials. In addition the thermal stability of the orthorhombic $TMA_2Sn_3Se_7$ phase is explored by *in situ* PXRD under nitrogen and in vacuum, from which it is determined that the structural integrity of the material is retained up to the point of template removal around 250 and 300 °C, respectively. With the available information it is possible to propose a modular assembly model to rationalize the formation of the observed microporous tin selenide phases.

Phase study: powder X-ray diffraction (PXRD)

Powder X-ray diffraction patterns were obtained on a Siemens D5000 diffractometer using a high-power Cu-Kα source (λ = 1.54178 Å) operating at 50 kV and 35 mA. A Kevex solid-state detector was used for energy dispersive discrimination of the Kβ component of the diffracted X-rays and for enhancing the signal to noise ratio. The samples were ground and packed into standard sample holders, 2 mm in depth, to minimize the effect of preferred orientation. For optimum comparison of samples they were run under identical experimental conditions; scan step 0.04° 2θ, 0.7 s per step within the 2θ range 2–50°, where the most informative reflections for these structures occur.

A time dependent phase study has been performed on the porous tin(IV) selenides. PXRD and single crystal X-ray diffraction techniques have been employed to monitor the progression of phases, which evolve over the period of a hydrothermal synthesis. It is established that products undergo a phase transformation from a two-dimensional orthorhombic to a two-dimensional monoclinic polymorph and eventually convert to a novel three-dimensional open-framework tetragonal phase.

In these experiments a total of 16 samples were prepared in a synthesis mixture with the stoichiometry: Sn : 2Se : TMAOH·$5H_2O$: $33H_2O$. The reaction mixtures were prepared using a procedure similar to that described previously.[24] This involved sequentially dissolving stoichiometric amounts of TMAOH·$5H_2O$ (tetramethyammonium hydroxide pentahydrate) in water in a 16 ml Enflon liner, selenium (elemental powder 99.5%, 100 mesh, Aldrich) and tin metal powder (elemental tin powder, 99.8%, 325 mesh, Aldrich). The reaction mixture was stirred for 5 min. The Enflon liners were sealed in stainless steel autoclaves and heated at 150 °C while tumbling. One reaction vessel was opened each day for a period of 16 days and the red crystalline product was washed with copious amounts of water and acetone and air-dried. A PXRD pattern of each product was recorded according to the protocols described earlier.[24]

For convenience of appraising the reaction profile data, PXRD patterns of 10 samples are displayed in Fig. 1(a) corresponding to the progression of events in the formation of these materials. Fig. 1(b) and (c) emphasize the emergence and disappearance of PXRD reflections in the range 2θ 6–12 and 9–12° respectively. The PXRD patterns shown in Fig. 1(a) and (b) suggest that several phases are formed and transformed over the time period of the reaction. At least four different phases have been identified, of which one occurs as a pure phase material at the initial (1 day) and one at the final

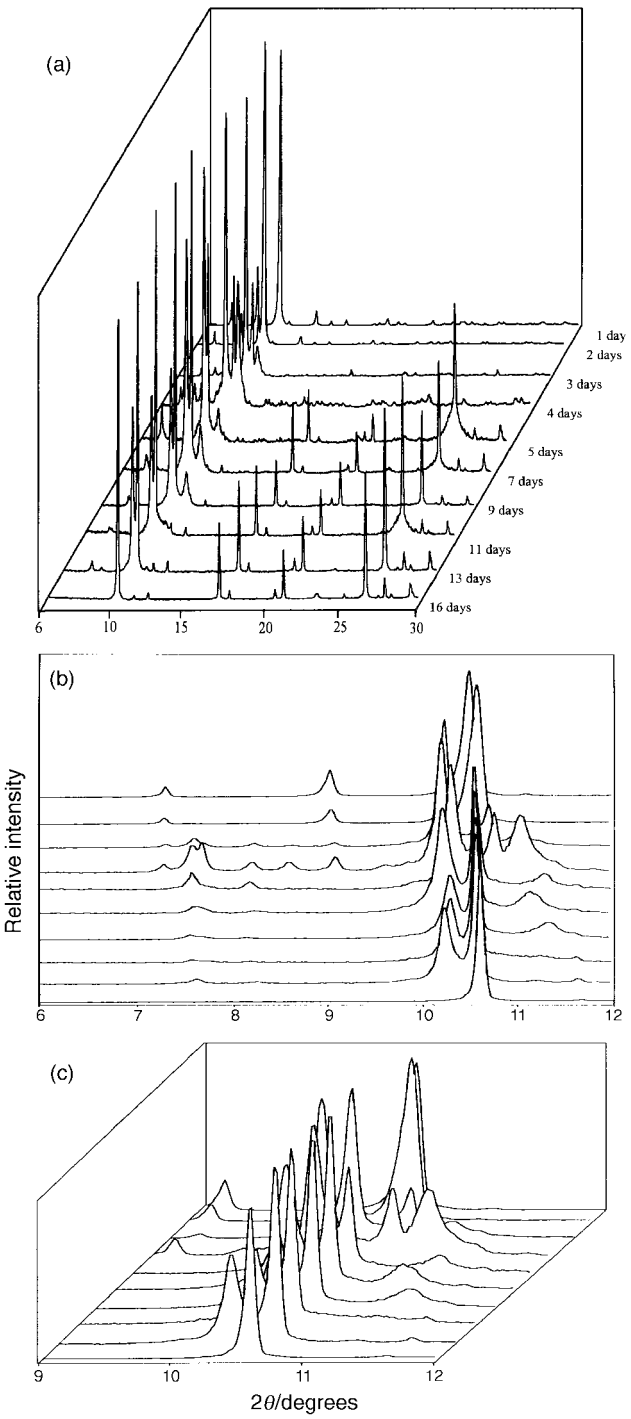

Fig. 1 (a) Powder X-ray diffraction patterns of ten samples with synthesis times ranging from one to 16 days, showing the existence of phase transitions between different porous tin selenide materials. (b) PXRD patterns of the time dependent phase transformations in the range 2θ = 6–12°. (c) PXRD patterns of the time dependent phase transformations in the range 2θ = 9–12°, emphasizing the changes in the most intense peaks.

(16 days) stages of the reaction. It has proven possible to obtain single crystal structures of three out of the four phases. The PXRD patterns suggest that after one day of reaction a pure orthorhombic phase is obtained. The crystals produced have hexagonal habits with their size ranging between 100 to 200 μm. The PXRD pattern of this phase is displayed in Fig. 2 along with the simulated powder pattern of this product obtained using the Cerius2[25] molecular simulation software. The extreme flexibility of this type of structure, especially along [010], is well known and described in detail in numerous

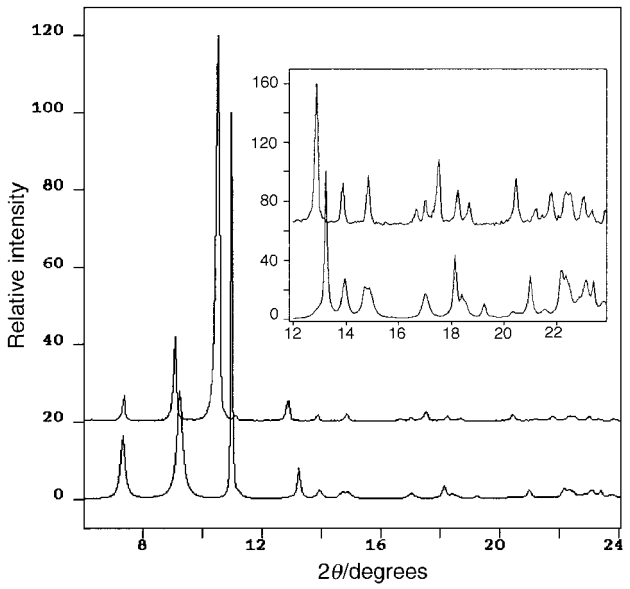

Fig. 2 PXRD pattern of the phase pure orthorhombic $TMA_2Sn_3Se_7 \cdot 1.5H_2O$ end-member (top) along with the simulated pattern (bottom) from the single crystal XRD structure produced using Cerius2[25] molecular simulation software. The insert displays an expanded region in the range $2\theta = 12$–24°.

of our previous papers.[26,27] The apparent differences between the two patterns in Fig. 2 is only due to the large difference in b_0 (which can take values from 16.03 to 16.86 Å) between the single crystal, used for the structure determination, and the bulk material analyzed by PXRD. The b_0 (that is the regular interlayer distance in the structure) was dramatically enlarged as a result of the mechanical treatment of this soft framework during sample preparation. Thus, not only the 020 reflection ($2\theta \approx 10.7^\circ$), but all other peaks with $k \neq 0$ should be affected with a different shift, depending on the value of k in their *hkl*-indices. These shifts toward smaller 2θ values of all reflections with $k \neq 0$ in Fig. 2 are indeed responsible for the apparent differences between the experimental and the simulated powder patterns. The identity between both diffraction patterns in Fig. 2 was confirmed by the whole pattern fitting refinement procedure using Powder Cell 2.0 software (W. Kraus and G. Nolse, 1998). The initial lattice parameters of the calculated pattern (the single crystal data are from Table 1) were refined against the experimental pattern in the iterative least squares procedure. At the end, both patterns completely matched each other and the refined lattice parameters a_0 and c_0 remain almost unchanged, while b_0 changed from 16.06 to 16.68 Å. The latter value is close to b_0 calculated for many other as-synthesized orthorhombic $TMA_2Sn_3Se_7$ samples that were ground and packed in the sample holders for routine PXRD analysis.

As previously reported, an increase of the interlayer spacing is also observed during NMR studies where the material is spun at 14 kHz and thus experiences high G forces.[24,26] Since the unit cell parameters in this particular phase are identical in two directions and vary in the third, it is suggested that the $TMA_2Sn_3Se_7$ product displays polytypism at various stages of the sample preparation/study.

After two days a well-defined shoulder emerges at 2θ *ca.* 10° corresponding to the monoclinic $TMA_2Sn_3Se_7$ phase. By the fourth day several peaks have appeared suggesting the coexistence of at least three phases in the product mixture. These correspond to the orthorhombic, monoclinic and a third phase whose identity is yet unknown. Fig. 3 displays the PXRD pattern of the products at this stage: the peaks that belong to orthorhombic and monoclinic phases after indexing and least squares fitting of the observed *d*-spaces are appropriately marked. The monoclinic crystals have hexagonal habits similar to their orthorhombic polymorphs. A fourth phase

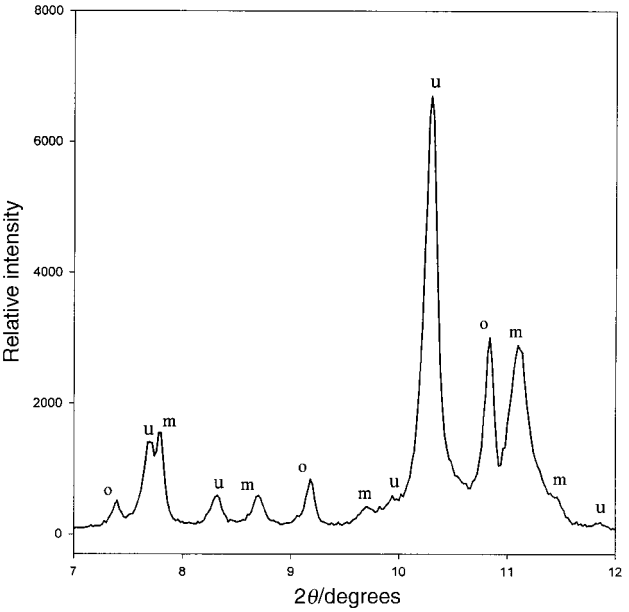

Fig. 3 Expanded region in the range $2\theta = 7$–12° of the PXRD pattern of the reaction products after four days. The coexistence of three phases is indicated by the notation of reflections: o = orthorhombic $TMA_2Sn_3Se_7$, m = monoclinic $TMA_2Sn_3Se_7$, u = unidentified phase.

Table 1 Single crystal XRD structure details for three product phases obtained in the tetramethylammonium templated tin(IV) selenide hydrothermal synthesis system

Compound	$TMA_2Sn_3Se_7 \cdot 1.5H_2O$	$TMA_2Sn_3Se_7 \cdot H_2O$	$TMA_2Sn_5Se_{10}O$
Empirical formula	$C_8N_2H_{27}Sn_3Se_7O_{1.5}$	$C_8N_2H_{26}Sn_3Se_7O$	$C_8N_2H_{24}Sn_5Se_{10}O$
Color, habit	Dark red, hexagonal plate	Red, hexagonal plate	Red cubo-orthorhombic blocks
Crystal size/mm	$0.3 \times 0.15 \times 0.15$	$0.2 \times 0.1 \times 0.2$	$0.1 \times 0.1 \times 0.1$
Crystal system	Orthorhombic	Monoclinic	Tetragonal
Space group	$P2_12_12_1$	$C2/m$	$I\bar{4}$
a/Å	13.675(2)	21.175(4)	9.909(1)
b/Å	16.062(4)	13.640(3)	9.909(1)
c/Å	24.067(4)	9.500(2)	15.161(2)
β/°		106.32(3)	
Volume/Å^3	5286(2)	2633(2)	1489(3)
Z	16	4	2
Formula weight	1081.1	1072.8	1547.3
D_c/g cm^{-3}	2.656	2.645	3.398
μ/mm^{-1}	24.91	12.495	16.366
λ(Mo-Kα)/Å	0.71073	0.71073	0.71073
F(100)	3888	1832	1320

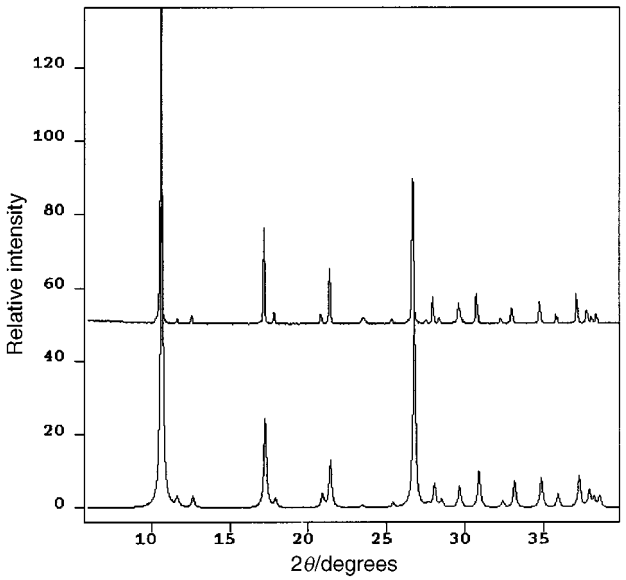

Fig. 4 PXRD pattern of the experimental (top) and simulated (bottom) tetragonal $TMA_2Sn_5Se_{10}O$, showing the phase purity of the product.

appears after 7 days corresponding to a tetragonal phase, which after heating for a total of 16 days becomes the sole phase to be observed. The crystals of this new phase are red with cubo-orthorhombic morphology. The PXRD pattern of this phase is shown in Fig. 4 and is compared to the simulated pattern based upon the single crystal structure confirming the phase purity of this product.

Single crystal X-ray diffraction structures

Structures of three of the four product phases have been determined using single crystal X-ray diffraction. Details of each structure are summarized in Table 1.

Full crystallographic details, excluding structure factors, have been deposited at the Cambridge Crystallographic Data Centre (CCDC). See Information for Authors, 1999, Issue 1. Any request to the CCDC for this material should quote the full literature citation and the reference number 1145/147.†

Fig. 5 and 6 display projections of the structures of the orthorhombic and monoclinic polymorphs of $TMA_2Sn_3Se_7$, respectively. These graphical images are produced using the Cerius2[25] molecular simulation software and present various perspectives of the porous layered structure of $TMA_2Sn_3Se_7$. Structures of both these polymorphs are based upon distorted trigonal bipyramidal $SnSe_5$ units connected together *via* a shared axial apex and three axial–equatorial edges to produce Sn_3Se_7 broken-cube clusters. Linkage of six of these broken-cube clusters through shared axial–equatorial Se atoms produces a planar honeycomb arrangement of 24-atom ring pores. Parallel stacking of these anionic $Sn_3Se_7^{2-}$ layers produces the porous layered $TMA_2Sn_3Se_7$ tin(IV) selenide. The layers in the orthorhombic phase are perpendicular to the [010] axis whereas in the monoclinic phase they pass through the $(20\bar{1})$ plane. As previously discussed[24] there are six crystallographically distinct tin atoms in the orthorhombic structure generating two different types of broken-cube clusters. However, there are only two distinct types of trigonal bipyramidal (*TBPY*) units in the monoclinic phase giving rise to a single type of broken-cube cluster. The *TBPY* units in the monoclinic phase are more symmetrical than their counterparts in the ortho-

†Although the structure of the monoclinic phase has been described here, details of its single crystal structure and data collection will be published separately as its structure has not yet been refined with a high enough degree of accuracy.

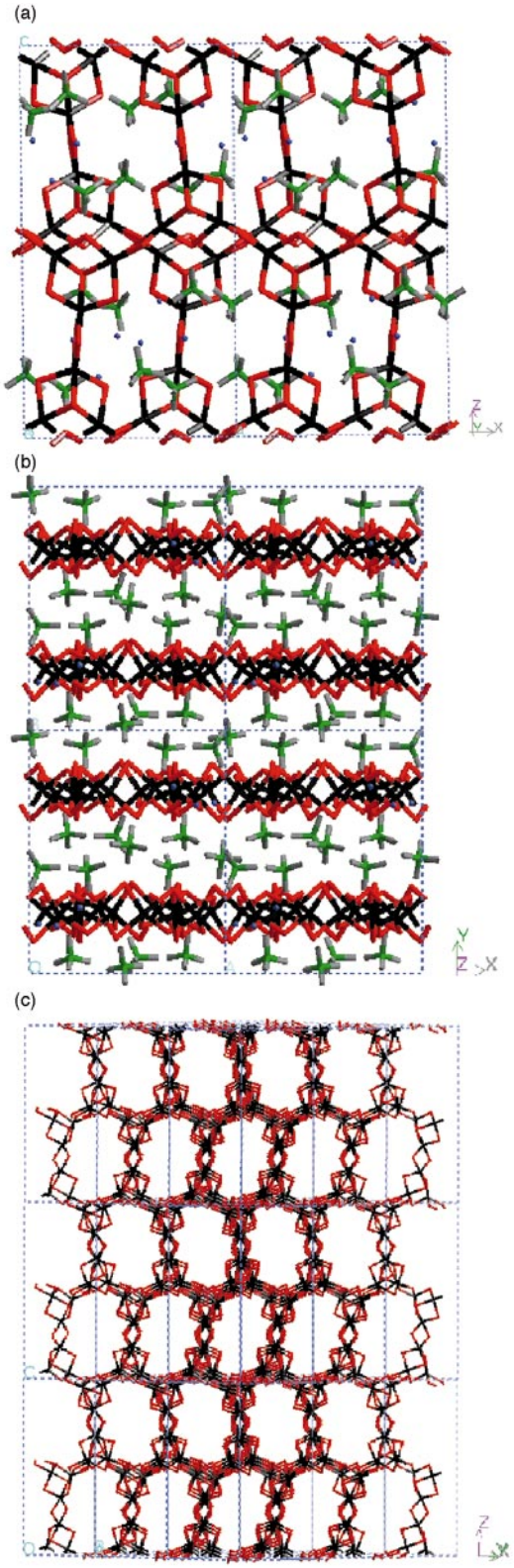

Fig. 5 (a) [010] projection of two unit cells of orthorhombic $TMA_2Sn_3Se_7 \cdot 1.5H_2O$ with $P2_12_12_1$ space group. Tin is black, selenium is red, oxygen is blue, nitrogen is green and carbon is gray. (b) [001] projection of four unit cells of orthorhombic $TMA_2Sn_3Se_7 \cdot 1.5H_2O$, displaying the layer planes of the structure. (c) Parallel stacking of the porous layers produces distorted hexagonal channels along the [110] axis with a center-to-center distance of *ca.* 14 Å. The organic template is omitted for clarity.

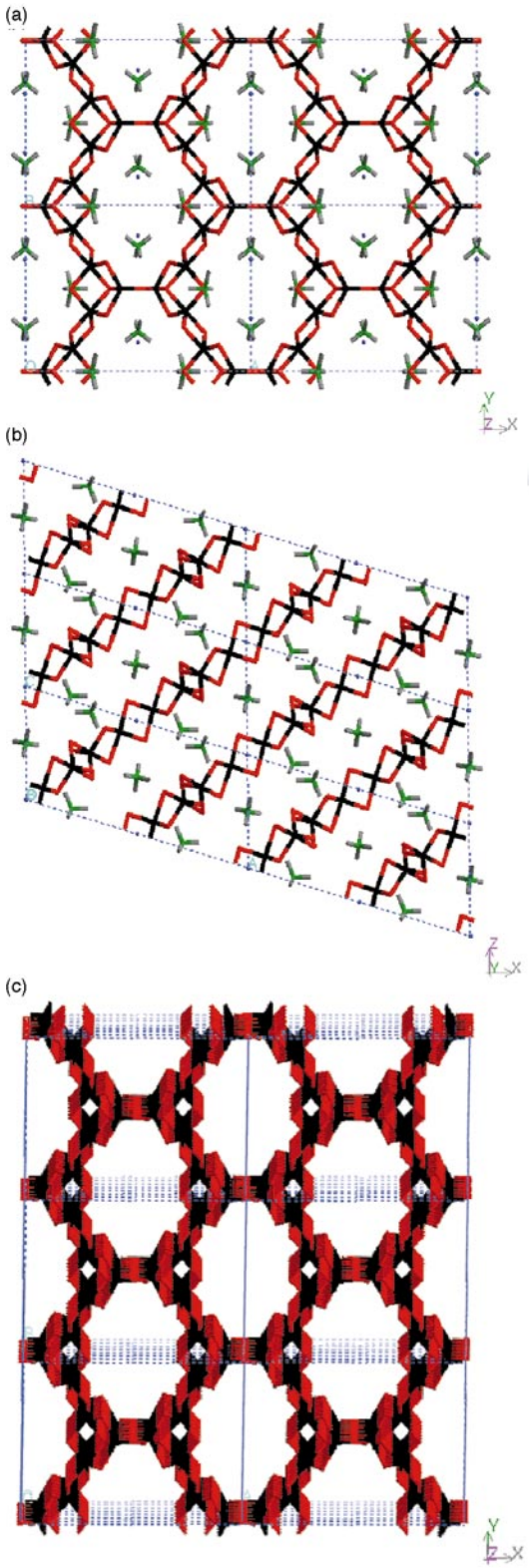

Fig. 6 (a) [001] projection of monoclinic $TMA_2Sn_3Se_7 \cdot H_2O$ and (b) [010] projection of six unit cells of monoclinic $TMA_2Sn_3Se_7 \cdot H_2O$. (c) Projection of several unit cells displaying the hexagonal channels along the [001] axis in monoclinic $TMA_2Sn_3Se_7 \cdot H_2O$. The template and water molecules are omitted for clarity.

rhombic phase. Similar to the orthorhombic phase, the five Sn–Se bond lengths in the monoclinic phase are slightly different, with the axial bonds being longer than the equatorial ones. However, unlike the orthorhombic phase the variation in length of the equatorial bonds is fairly minimal. The important bond lengths and bond angles of the orthorhombic phase are included in CCDC 1145/147.

Comparison of the layered structure of these two phases in Fig. 7 reveals several major differences. The structure of the orthorhombic polymorph with space group $P2_12_12_1$ contains three hydrogen-bonded water molecules per 24-atom ring, positioned off-center and in close proximity to three of the six Sn_3Se_7 clusters. The 24 atoms form a pore with a distorted hexagonal shape. There are four TMA^+ cations around each Sn_3Se_7 broken-cube cluster building unit. One of the TMA^+ cations is arranged in such a way that it points into the open side of the broken-cube cluster, replacing the missing apex of the cube, and oriented in a staggered fashion with respect to the three capping bonds of the selenium atom. In contrast, the monoclinic phase with space group $C2/m$ displays regular hexagonal shaped pores. Similar to the orthorhombic phase, there are four TMA^+ cations positioned around each Sn_3Se_7 broken-cube cluster. However, the cation pointing into the missing apex of the broken-cube is arranged in an eclipsed

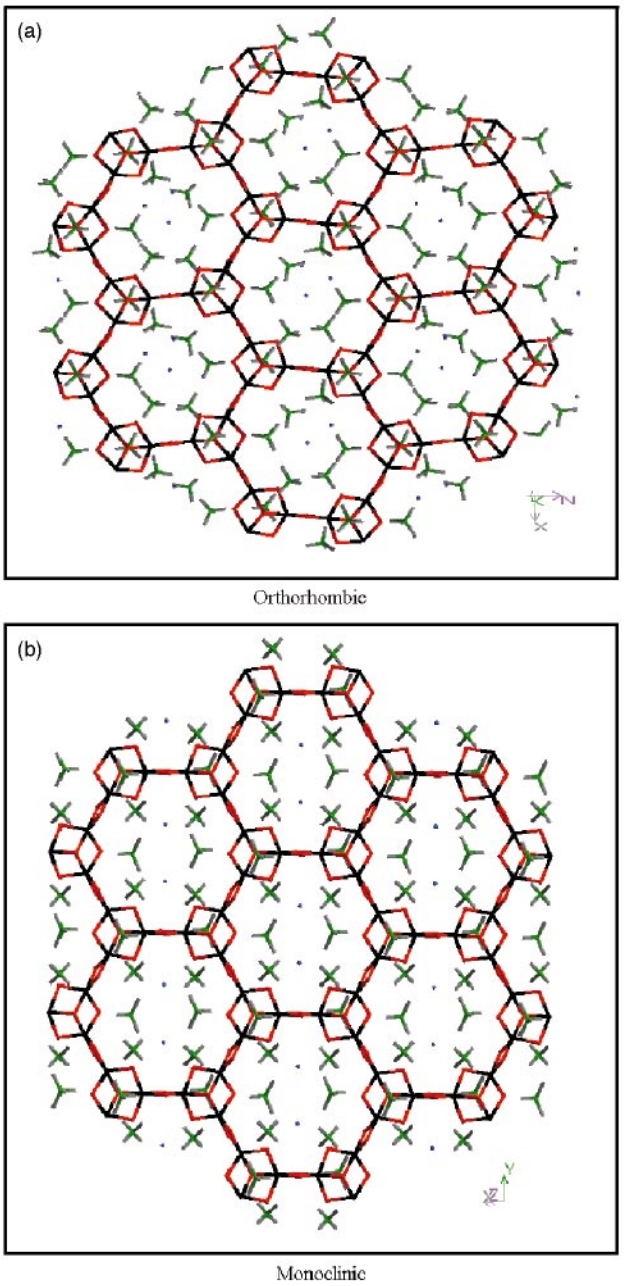

Fig. 7 Comparison of layer and template architecture in the orthorhombic (top) and monoclinic (bottom) polymorphs of $TMA_2Sn_3Se_7$, displaying the structural differences between the two materials.

fashion with respect to the three capping bonds in the broken-cube cluster. There are two water molecules per 24-atom ring, well separated and positioned symmetrically with respect to the center of the pore. In this phase the pores have a free diameter of *ca.* 10.93 Å and a center-to-center distance of *ca.* 13.64 Å which is slightly smaller than the orthorhombic phase. Fig. 8 differentiates schematically between the 24-atom hexagonal pores in the orthorhombic and monoclinic phases. The bond angles between three capping selenium ($\angle U_2D_3U_4$, where U and D denote broken-cube clusters with their capping selenium respectively up and down) atoms and the distances between the facing Se caps ($d\,U_2D_5$) have been used to quantify the differences between the hexagonal pore architecture of these two polymorphs.

The extent of the guest loading in these flexible porous layered host materials has a significant effect on the symmetry of the pores and the organization of their layers. This is demonstrated by the structures of the two polymorphs described in this study, as well as the earlier reported variation in the unit cell parameters of members of the family of porous layered tin sulfides, upon reversible adsorption-desorption of physisorbed water.[21–23,26] It appears that by changing the number of guest water molecules from just three to two within the pores, the entire framework of these materials flexes in order to satisfy the new spatial constraints. This is achieved by a cooperative displacement of the template cations, waters and porous layers resulting in more symmetrical 24-atom rings and a new arrangement of the guests. Furthermore, the template cation can determine the space group and lattice type of the final product. This finds support in the structure of the reported monoclinic cesium analogue $Cs_2Sn_3Se_7$[28] and

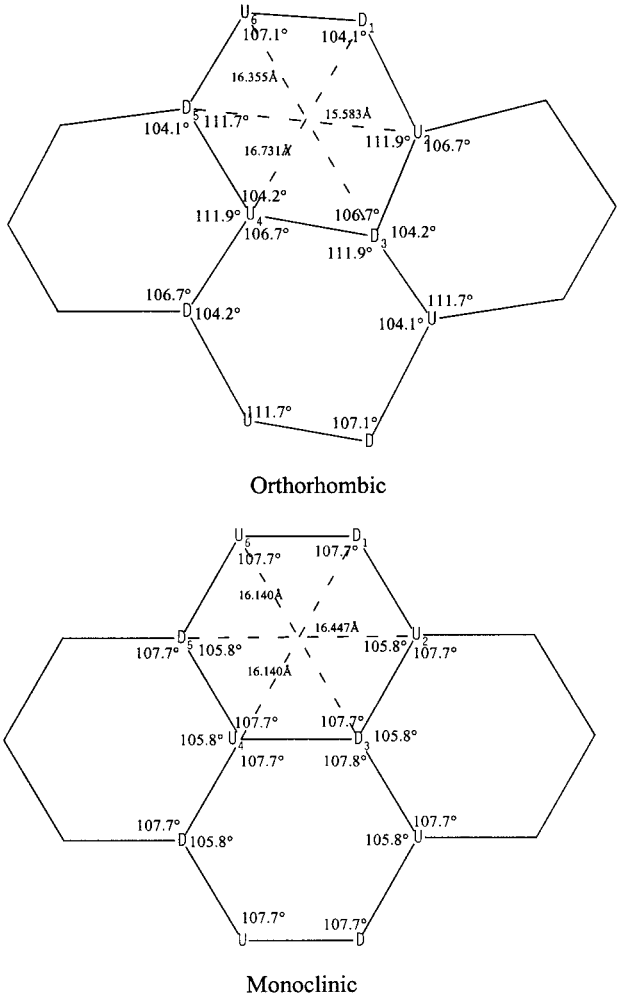

Fig. 8 Illustration of the layer geometries of the orthorhombic (top) and monoclinic (bottom) $TMA_2Sn_3Se_7$ materials. The bond angles between three capping selenium atoms with an up and down configuration ($\angle U_2D_3U_4$) and the distances between the facing caps (dU_2D_5) emphasize the differences in hexagonal pore symmetry within the layer planes of these materials.

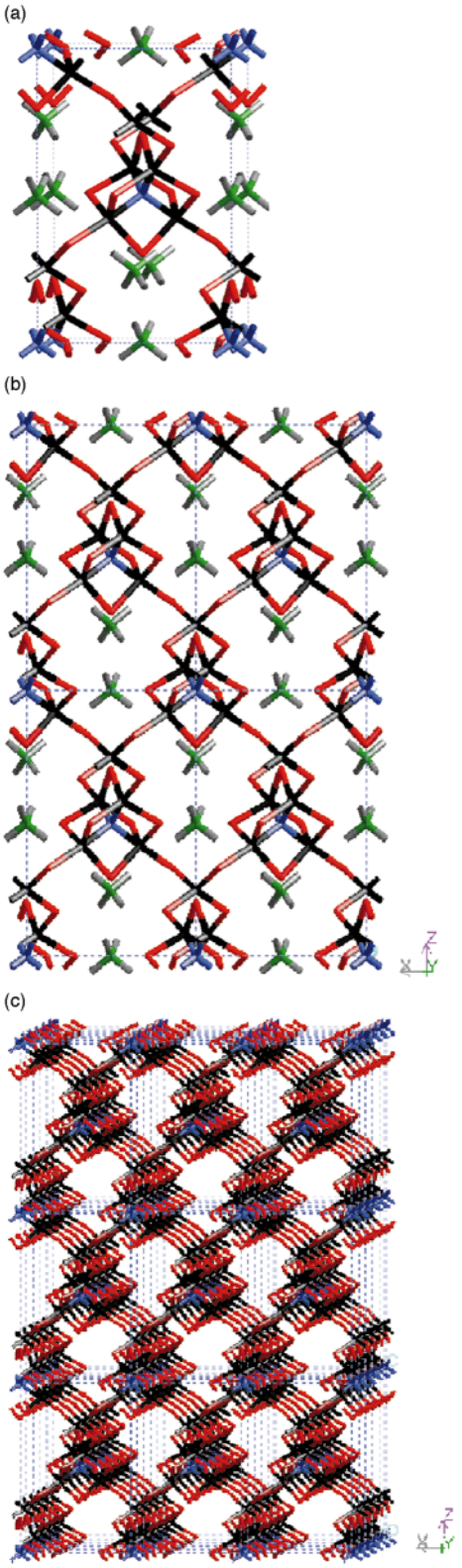

Fig. 9 (a) Single crystal XRD structure of the tetragonal $TMA_2Sn_5Se_{10}O$. (b) $Sn_4Se_{10}O^{6-}$ adamantanoidal units connect to one another through a tetrahedral $SnSe_4$ bridge to create a porous structure. (c) View of the channels in the framework structure of $TMA_2Sn_5Se_{10}O$ along the [010] axis. The organic cations are omitted for clarity.

the orthorhombic $R_2Sn_3Se_7$ phase synthesized using triethylenetetramine as the template.[29]

After passing through the emergence and disappearance of $TMA_2Sn_3Se_7$ polymorphs and a yet unknown phase, the final pure phase product appears after 5 days of reaction time. It is worth noting that this phase is the only observed phase even after 23 days of reaction. The structure of this phase has been solved by single crystal XRD and found to be a novel three-dimensional open-framework, Fig. 9. The structure consists of adamantane-like selenostannate building blocks $Sn_4Se_{10}O^{6-}$ having an endohedral oxygen uniquely located at the center of the cluster. These building blocks are connected to four neighboring $Sn_4Se_{10}O$ clusters *via* pseudo-tetrahedral μ_4-$SnSe_4$ tin selenide units sharing the terminal selenides, Fig. 9(a). This connection produces the three-dimensional open framework structure shown in Fig. 9(b). The open framework has a zinc blende-type of expanded lattice such that each zinc atom in the zinc blende is replaced with a tetrahedral $SnSe_4$ cluster and a $Sn_4Se_{10}O$ cluster replaces each sulfur. This porous material contains channels along the [010] axis, Fig. 9(c), with a free diameter (omitting the template) of 9.642×6.888 Å and a centre-to-centre diameter of 9.642 Å. There are two TMA^+ templating cations residing within the void spaces.

In group 14 metal chalcogenides, adamantane-like clusters are well known. Molecular species such as $(MeSn)_4Se_6$,[30] $TMA_4Ge_4S_{10}$,[31,32] $Na_4Ge_4S_{10}$, $Ba_2Ge_4S_{10}$, $Na_4Si_4S_{10}$,[33] $TMA_4Ge_4Se_{10}$,[34,35] $TMA_4Sn_4S_{10}$[35,36] and $TMA_4Sn_4Se_{10}$[35,36] are all reported to have an adamantane-type structure. However, the only known adamantane-like cluster to have endohedral oxygens within the cages is $Sn_{10}O_4S_{20}^{8-}$, which is described as a supertetrahedral polyanion built from ten corner sharing SnS_4 tetrahedra. Four oxygen atoms are inserted in the tetrahedral voids to complete the coordination of six of the ten Sn atoms to produce distorted SnS_4O_2 octahedra.[37,38]

The rate of formation and transformation of these three phases appears to be highly dependent on the reaction temperature. It has been determined that at 158 °C the tetragonal phase is obtained after 5 days in such a way that the orthorhombic phase directly transforms to the tetragonal phase apparently by-passing the monoclinic phase. This suggests that the different phases are not stable at all temperatures.

The order of phase transitions in the synthesis of the porous tin(IV) selenides observed in this study appears to follow Oswald's law of successive reactions. This implies that the initially formed orthorhombic product is thermodynamically less stable than the succeeding phases. The two-dimensional orthorhombic phase is initially transformed to a two-dimensional monoclinic polymorph and later to a three-dimensional tetragonal phase suggesting that the latter two have lower free energies. The most stable phases in the system actually appear to be the elemental forms of selenium and tin metal, and $SnSe_2$. These dense materials are most likely the result of air oxidation and structure collapse. It is fairly safe to suggest that the first orthorhombic to monoclinic transition is a polymorphic displacive transformation caused by the guest water-induced distortion of Sn–Se bonds. However, the subsequent conversion of the monoclinic to the tetragonal phase, where the structure is transformed from a two-dimensional layered to a three-dimensional open-framework, involves breakage and reformation of Sn–Se bonds making it a 'non-polymorphic' reconstructive transformation.

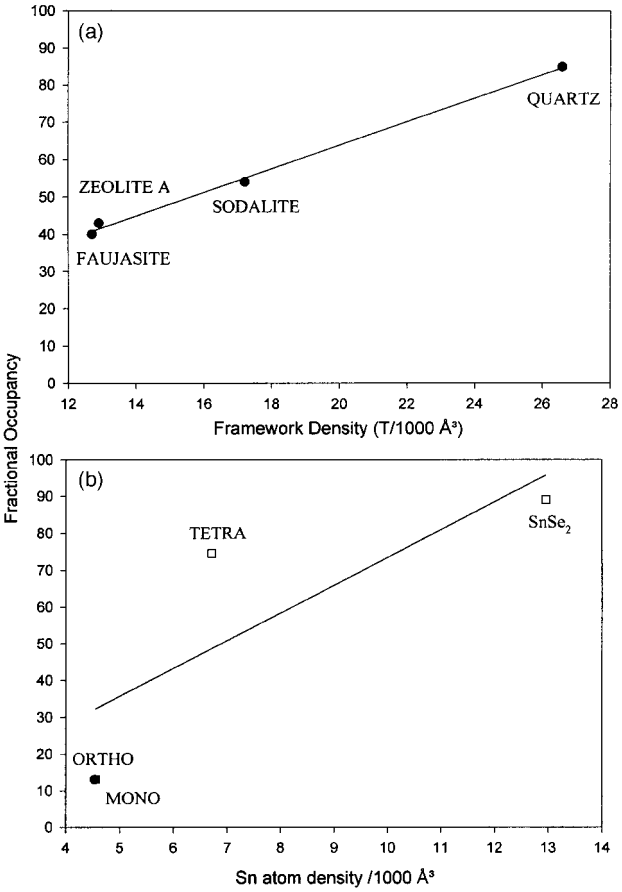

Fig. 10 Relationship between the fractional occupancy and the framework density of the unit cell of (a) zeolites and (b) porous tin(IV) selenides.

Comparison of the observed interconversions for the microporous tin(IV) selenides of this study with zeolites reveals an interesting similarity. When synthesizing aluminum rich zeolites from an alkali metal aluminosilicate gel, Oswald's law of successive reactions is observed.[5,8] For example, in a hydrothermal synthesis, zeolite A (FD = 12.9 T/1000 Å^3) is transformed to sodalite (FD = 17.2 T/1000 Å^3) and eventually to carnegieite (FD = 26.25 T/1000 Å^3), the $NaAlSiO_4$ composition of stuffed cristobalite. Thus, the reaction proceeds to yield materials with increasing framework density.[5,8,39] The fractional occupancy of a solid state material is defined as the ratio of the occupied volume divided by the total volume of the unit cell. This has been determined earlier for these zeolites by calculating the Connolly[40,41] surfaces of the frameworks. The calculation provides the total and the available volume from which the total occupied volume of the unit cell is obtained. Fig. 10(a) displays a monotonic relation between the fractional occupied volume of the unit cell and the T-atom

Table 2 Summary of the calculated volumes and framework densities of the unit cells for porous tin(IV) selenide materials including the template and the water molecules. The values are calculated using the Connolly surface package of the Cerius2[25] molecular simulation software, with a probe radius of 0.5 Å

Product	Total unit cell volume/Å^3	Total available volume/Å^3	% Fractional occupancy	Framework density (Sn/1000 Å^3)
Ortho-$TMA_2Sn_3Se_7$	5286.26	4597.74	13.025	4.54
Mono-$TMA_2Sn_3Se_7$	2633.57	2289.34	13.071	4.56
Tetra-$TMA_2Sn_5Se_{10}O$	1488.63	379.47	74.51	6.717
$SnSe_2$	77.19	8.43	89.08	12.96

framework density for these zeolites. (Quartz with comparable framework density (FD = 26.6 T/1000 Å^3) to carnegieite is used as the reference for the dense end product).

Table 2 summarizes the observed unit cell volumes and calculated framework densities of the porous tin(IV) selenide materials described in this study (note, the templates and water molecules are included). It is particularly interesting that the order of appearance and decay, in the hydrothermal synthesis of these phases, parallels the fractional occupancy and framework density of the unit cell, Fig. 10(b). Note that the framework density (FD) in the porous selenides is defined as the number of tin atoms per 1000 Å^3. The observation of successive transformations amongst the porous selenides may be the first time that the Oswald rule has been found to apply to non-oxide open-framework materials. In summary, it appears that by analogy with faujasite, zeolite A, sodalite and carnegieite, the tetramethylammonium-templated hydrothermal reaction of the tin selenides progresses from the least dense orthorhombic $TMA_2Sn_3Se_7$ to a slightly more dense monoclinic $TMA_2Sn_3Se_7$ to a denser tetragonal $TMA_2Sn_5Se_{10}O$. Although $SnSe_2$ is not the end phase under reaction conditions, it is used as the most dense reference phase.

Fig. 11(a)–(c) display the calculated Connolly surfaces for the three porous tin(IV) selenide products, graphically revealing the available space along the channels upon removal of the templates and water. The amount of available void space decreases from the orthorhombic to the tetragonal product.

An observation which is worth mentioning is that the tetragonal phase is not obtained in the sulfur system, perhaps due to the smaller covalent radius of the sulfur, and the ring and cage strain that are expected to influence the stability of this structure. Further study is required to understand the structural and mechanistic details of the phase transformations in porous tin chalcogenide materials.

High temperature powder X-ray diffraction

In situ variable temperature powder X-ray diffraction patterns for the orthorhombic $TMA_2Sn_3Se_7$ material, shown in Fig. 12, were recorded under a nitrogen atmosphere. Several changes are noted in the patterns. Upon heating, the material retains its crystallinity up to 170 °C. There is a gradual increase in the value of the interlayer spacing (020 reflection in Fig. 12(b), $2\theta \approx 10.5°$), as a result of the thermal expansion of the unit cell. From 170 to 230 °C the intensity of the reflections deteriorate with a further shift of the 020 reflection to higher *d*-spacing. The unit cell stops expanding at around 230 °C after an increase of *ca.* 0.3 Å from the initial interlayer spacing of the material. From 230 to 270 °C it appears that the organic guest begins to react with the framework with a concomitant contraction of the interlayer spacing. This is apparent from the shift of the interlayer spacing to lower *d*-values. Above 270 °C the template is completely lost and the framework collapses followed by formation of an amorphous $SnSe_2$ phase as seen in Fig. 12(a).

From analogous high temperature *in situ* PXRD studies of the tin(IV) sulfides it has been determined that the framework of these materials is stable to > 300 °C under vacuum compared to 230 °C under nitrogen. It is believed that under vacuum, the cracking products are removed faster giving them less opportunity to react with the framework, thereby enhancing the thermal stability of the framework.[20,42]

Modular assembly formation pathway

The accumulated knowledge acquired from the work done on porous tin(IV) selenides and earlier sulfide systems, in addition to the body of information available from the literature, has made it possible to formulate a model for the formation of the observed phases. The similarities between the sulfur and

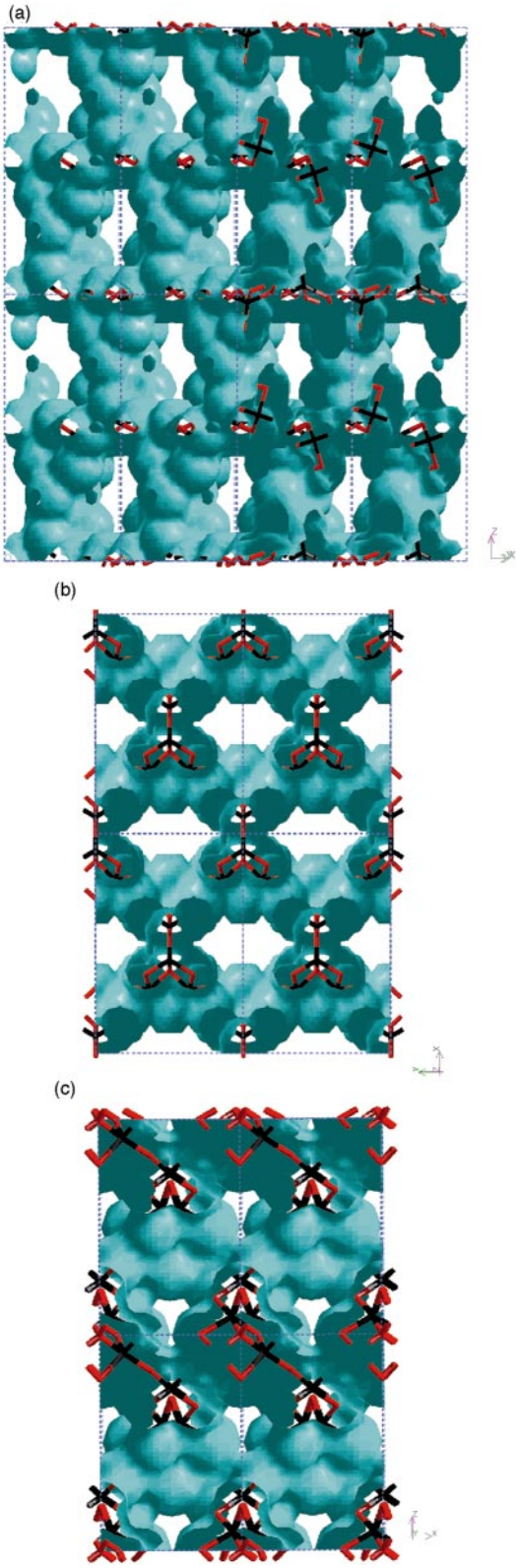

Fig. 11 (a) Connolly surface representation of orthorhombic $TMA_2Sn_3Se_7$ without the template and water molecules, displaying the void space in the framework. The image is generated using Cerius2[25] molecular simulation software with a probe radius of 0.5 Å. (b) Connolly surface representation of monoclinic $TMA_2Sn_3Se_7$ without the template and water molecules, displaying the void space in the framework. The image is generated using Cerius2[25] molecular simulation software with a probe radius of 0.5 Å. (c) Connolly surface representation of tetragonal $TMA_2Sn_5Se_{10}O$ without the template, displaying the void space in the framework. The image is generated using Cerius2[25] molecular simulation software with a probe radius of 0.5 Å.

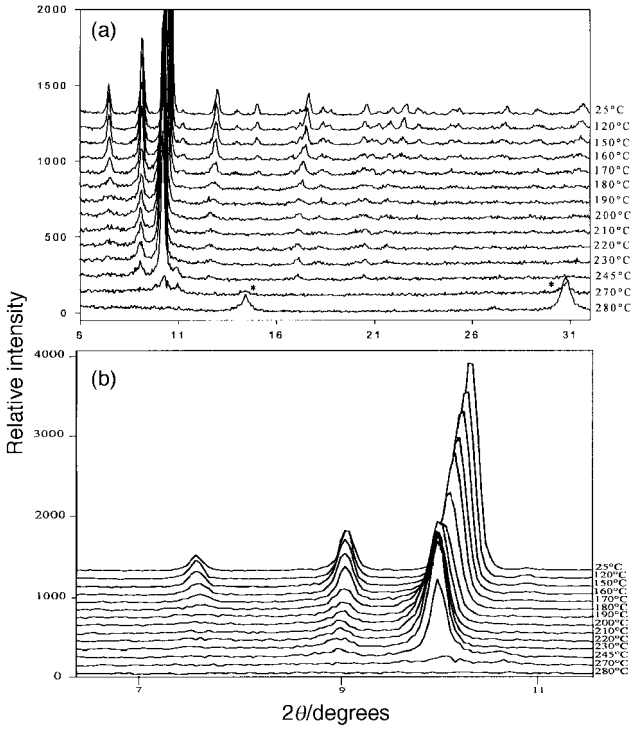

Fig. 12 (a), (b) High temperature powder X-ray diffraction patterns, collected under a nitrogen atmosphere for the orthorhombic TMA-SnSe-1. *$SnSe_2$.

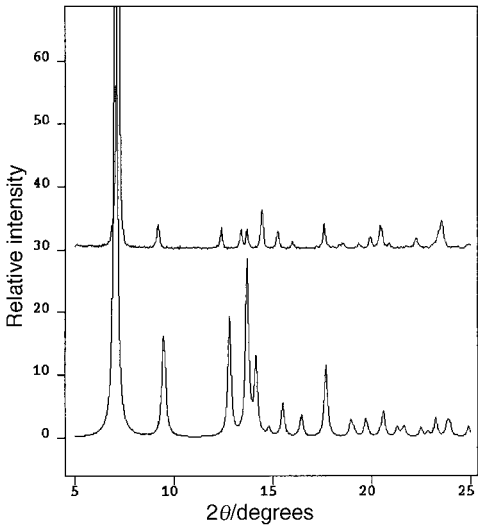

Fig. 13 PXRD patterns of $(C_6H_{11}NH_3)_4Sn_2Se_6$ (top) and the simulated pattern of its $Sn_2S_6^{4-}$ analogue (bottom) created using Cerius2[25] molecular simulation software. The patterns indicate the isostructurality of the two compounds.

selenium systems proved advantageous since the toxicity and the odorous nature of the selenium products, especially in the solution phase, restricted the methods available for their safe analysis.

It has been demonstrated that in the hydrothermal synthesis of porous tin(IV) sulfides several molecular species coexist in the mother liquor at different stages of the reaction.[43] Knowledge of the existence and the structures of these species is an important asset in understanding the chemistry occurring in the hydrothermal synthesis of these materials. ^{119}Sn NMR studies of the mother liquors of several porous tin(IV) sulfide materials have established the presence of monomeric SnS_4^{4-} (tetrathiostannate) and dimeric $Sn_2S_6^{4-}$ (hexathiodistannate) species in the solution.[43] The dimer species has been crystallized from the mother liquors, and the identity of the monomer and dimer have been confirmed by comparison of their NMR and UV–VIS absorption spectra with those of known species. Anionic tetrathiostannates are well known and characterized.[44,45] $Sn_2X_6^{4-}$ dimers (X = S, Se) are known to form with variety of cations.[46–48]

The $Sn_2S_6^{4-}$ dimer has been synthesized hydrothermally in this work using elemental Sn and S and either cyclohexylamine (denoted as $C_6H_{11}NH_2$ = CHA)[21,43] or tetramethylammonium hydroxide pentahydrate[49] as the organic template. To show the similarity between the sulfur and selenium systems, the selenium analogue of the dimer has also been synthesized under hydrothermal conditions using cyclohexylamine as the organic template at 150 °C following the reaction stoichiometry: $Sn:3Se:4C_6H_{11}NH_2:30H_2O$ the protonated $C_6H_{11}NH_3^+$ (denoted as CHAH) dimer crystals are green and have a needle shape morphology. Fig. 13 displays the PXRD patterns of the $Sn_2Se_6^{4-}$ (hexaselenodistannate) product and its comparison to the simulated PXRD pattern of its $Sn_2S_6^{4-}$ analogue, both of which were synthesized according to the reaction stoichiometry above. As anticipated, several reflections have shifted as a result of differences between the unit cell parameters of the two compounds. It is evident however that the materials are isostructural. The structure of the $(CHAH)_4Sn_2Se_6$ dimer has been determined using single crystal X-ray diffraction. The structure details are summarized in Table 3 and are compared to that of $(CHAH)_4Sn_2S_6$.[21] Fig. 14 displays a unit cell representation of the dimer. The compound crystallizes in the monoclinic $C2/c$ space group with the dimer structure based on edge sharing of two $SnSe_4$ tetrahedral units. Four cyclohexylammonium cations are located in close proxim-

Table 3 Summary of the single crystal XRD structures of the $(C_6H_{11}NH_3)_4Sn_2Se_6$ dimer and $TMA_2Sn_4Se_{10}$ tetramer

Compound	$(C_6H_{11}NH_3)_4Sn_2Se_6$	$(C_6H_{11}NH_3)_4Sn_2Sn_6$[21]	$TMA_2Sn_4Se_{10}$
Empirical formula	$C_{24}H_{56}N_4Sn_2Se_6$	$C_{24}H_{56}N_4Sn_2Sn_6$	$C_{15.875}N_{3.875}H_{48}Sn_{3.875}Se_{9.875}$
Color, habit	Green needles	Yellow needles	Dark yellow cubes
Crystal size/mm	$0.21 \times 0.24 \times 0.41$	$0.23 \times 0.21 \times 0.18$	$0.3 \times 0.25 \times 0.3$
Crystal system	Monoclinic	Monoclinic	Cubic
Space group	$C2/c$	$C2/c$	$P4\bar{3}n$
a/Å	26.145(5)	26.861(5)	20.545(2)
b/Å	7.765(2)	7.4660(10)	
c/Å	21.015(4)	20.109(4)	
β/°	114.636(12)	111.14(3)	
Volume/Å^3	3878(1)	3761(1)	8672(2)
Z	4	4	8
Formula weight	1111.18	830.47	1533.0
D_c/g cm^{-3}	1.904	1.467	2.348
μ(MoKα)/mm^{-1}	6.938	1.680	10.510
λ(Mo-Kα)/Å	0.71073	0.71073	0.71073
F(000)	2128	1696	5599

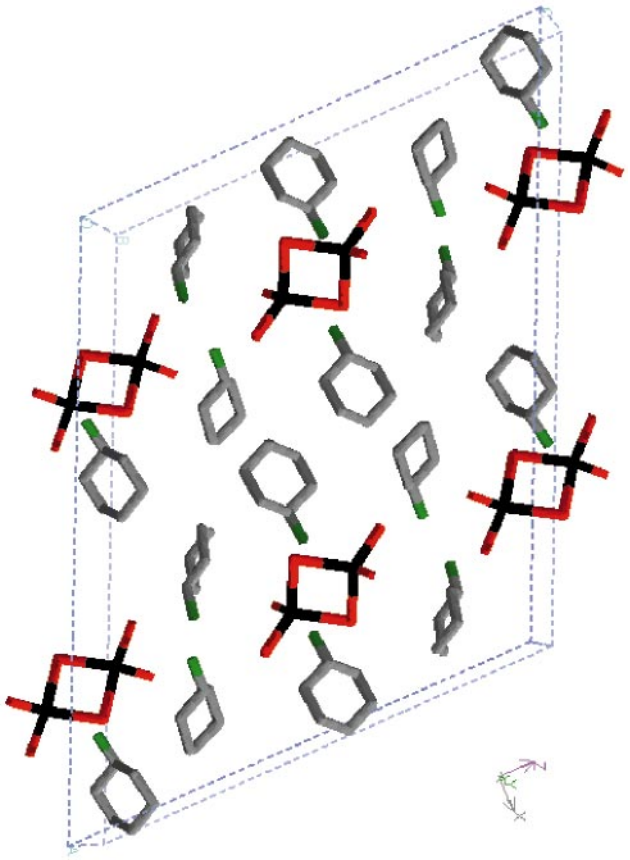

Fig. 14 Unit cell representation of $(C_6H_{11}NH_3)_4Sn_2Se_6$ created using the Cerius 2^{25} molecular simulation software.

ity and within hydrogen bonding distances to the terminal selenium atoms.

Another molecular species has also been identified in the hydrothermal synthesis of the microporous tin(IV) selenides. Adamantanoid $TMA_2Sn_4Se_{10}$ crystallizes in very small quantities at the final stages of the reaction (after 12 days). The crystals have been structurally characterized using single crystal X-ray diffraction as having a cubic unit cell with $P\bar{4}3n$ space group. Fig. 15 displays the PXRD pattern of this compound and its comparison to the simulated powder pattern produced using Cerius2[25] software. Fig. 16(a) shows a tilted unit cell

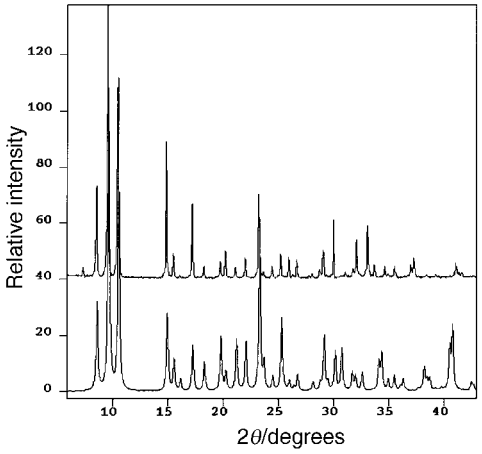

Fig. 15 PXRD patterns of $TMA_4Sn_4Se_{10}$ (top) and simulated pattern produced from the single crystal XRD structure using Cerius2[25] molecular simulation software. The differences observed at the high 2θ region are possibly due to disorder in the template positions in the crystals. An extra peak at $2\theta \approx 8^\circ$ likely belongs to a small amount of crystallized dimer in the sample.

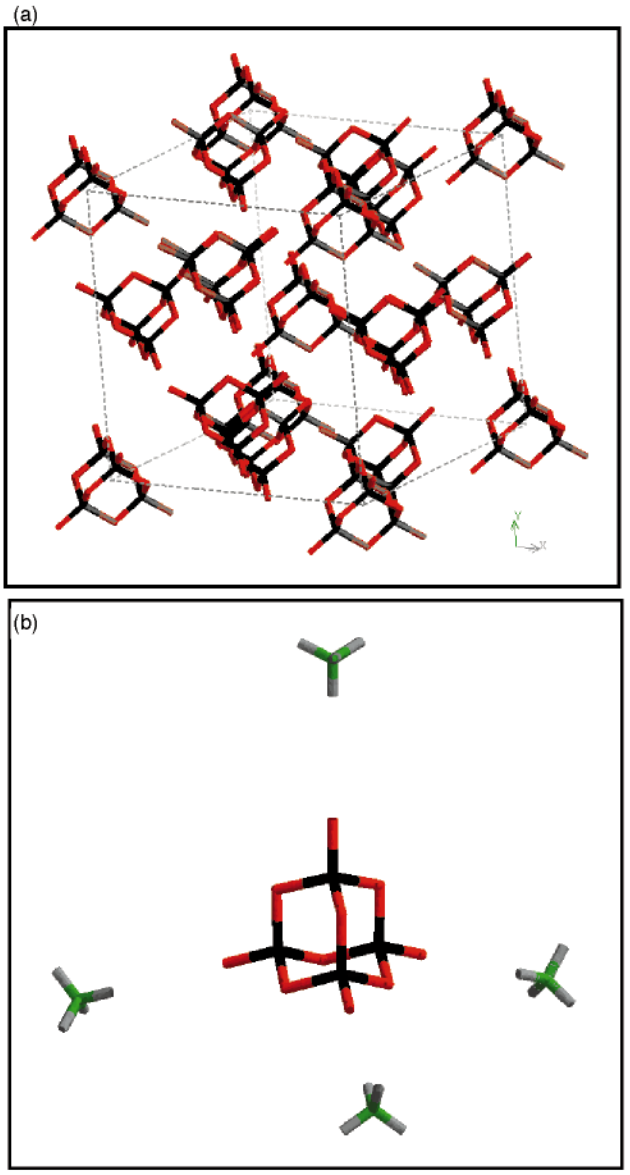

Fig. 16 (a) Unit cell representation of cubic $TMA_4Sn_4Se_{10}$ produced using Cerius2[25] molecular simulation software. Templates are omitted for clarity. (b) Cerius2[25] molecular simulation representation of a adamantanoidal $TMA_4Sn_4Se_{10}$ cluster.

representation of the $TMA_2Sn_4Se_{10}$ adamantane-like tetramer and Fig. 16(b) displays an individual $TMA_4Sn_4Se_{10}$ cluster. Four TMA^+ cations are located around each adamantanoid cluster in close proximity to the terminal selenium atoms. The details of the structure of the tetrameric cluster are summarized in Table 3. Information on the data collection, atomic coordinates and important bond lengths and angles for both of these compounds are given in CCDC 1145/147. It is worth noting that although the sulfur analogue of the tetramer species has not been identified from the reaction mixture that produces the microporous tin(IV) sulfides, it has been independently synthesized by other routes and its structure solved.[35,36,49,50]

It has been established from this work and the work of others that the synthesis and isolation of different phases of microporous tin sulfides and selenides is highly dependent on the temperature, reactant concentration and most importantly, the pH of the starting and the final solutions. At high values of pH, around 13 to 14, the dominant species in the solutions are the SnX_4^{4-} monomer and $Sn_2X_6^{4-}$ dimer (X = S, Se). As the pH gradually drops through condensation–polymerization of the tetrahedral SnX_4^{4-} species, higher oligomers such as the tetramer and the $Sn_{10}O_4S_{20}^{8-}$ materials form.[37,38,44] Indeed

it appears in the microporous tin(IV) selenide system that the crystals of the $Sn_4Se_{10}^{4-}$ tetramer form after the pH of the solution drops to around 9. It has also been established from the microporous tin(IV) sulfide and selenides that if the pH of the starting reaction mixture is reduced to around 10, bulk SnS_2 and $SnSe_2$ materials form, respectively.[34,43]

Scheme 1 displays a proposed reaction pathway for the formation of two-dimensional microporous layered and three-dimensional open framework tin(IV) selenide materials *via* a modular assembly route. It is suggested that at the high starting pH conditions of the hydrothermal Sn–Se–TMAOH–H_2O synthesis mixture, the dominant solution phase species are $SnSe_4^{4-}$ and $Sn_2Se_6^{4-}$, the latter being more abundant. As the pH of the solution drops and the solution becomes more acidic, there is an increase in the degree of protonation of the selenostannate anions. A ^{119}Sn NMR study of the mixed orthorhombic $TMA_2Sn_3S_xSe_{7-x}$ phase suggested that the dimers could link together to form the broken-cube cluster that is the basic construction unit of the two-dimensional orthorhombic and monoclinic $TMA_2Sn_3Se_7$ materials.[24] This is believed to be the result of the condensation-polymerization of Sn–SeH bonds with concomitant formation of H_2Se and progressive decrease in the pH of the reaction mixture from its initial value of *ca.* 14.3 to its final value of *ca.* 9.3. Coordination of $SnSe_4^{4-}$ ligands to a decapped Sn_3Se_6 broken-cube cluster provides a possible entry to the adamantanoid $Sn_4Se_{10}^{4-}$ cluster as sketched in Scheme 1. So far, the hypothetical Sn_3Se_6 species has not been isolated from these reaction mixtures perhaps as a result of its rapid coordination to $SnSe_4^{4-}$ monomers. A molecular compound has however, been reported with the formula of $Me_6Sn_3S_3$ where methyl groups can be considered to have replaced the bridging chalcogenide atoms of the Sn_3Se_6 cluster.[51] Furthermore, coordination of a $SnSe_4^{4-}$ monomer to an oxide-capped $Sn_3Se_6O^{2-}$ broken-cube cluster could produce the selenostannate $Sn_4Se_{10}O^{6-}$ unit. These clusters in the presence of $SnSe_4^{4-}$ species can be envisaged to link together to form the three-dimensional $Sn_5Se_{10}O^{2-}$ open framework structure, Scheme 1. In addition, dissociation of the capping Se in $TMA_2Sn_3Se_7$ as a result of the decrease in the pH would produce a neutral layer plane of Sn_3Se_6 followed by loss of two charge-balancing TMA^+ cations.

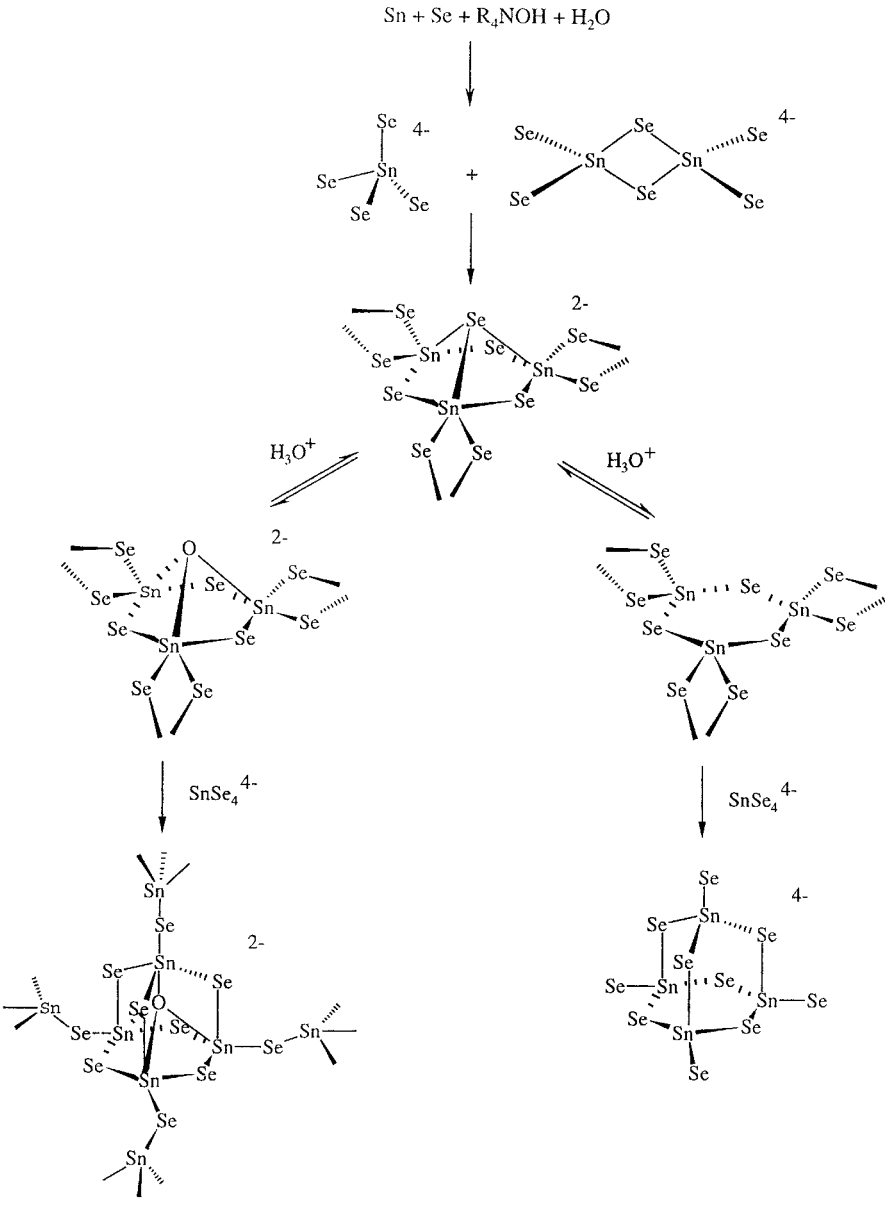

Scheme 1 Proposed model for the formation of two-dimensional layered and three-dimensional open framework tin(IV) selenides *via* a modular assembly reaction pathway.

This could result in exfoliation of the layers from the crystals. If this were the case, layer-by-layer reactions would effectively mineralize the $TMA_2Sn_3Se_7$ material into a form that is favorable for reaction with the species present in the solution namely, H_3O^+ and $SnSe_4^{4-}$. This idea could also be useful in explaining the formation of other two-dimensional layered and three-dimensional open frameworks.

Conclusion

It has been established in this study that the hydrothermal reactions that create two-dimensional microporous layered and three-dimensional open-framework tin(IV) selenide materials behave thermodynamically like zeolites. That is to say, over time and at a constant temperature several materials form and transform from less to more dense structures, implying the existence of metastable phases. Four phases have been identified in the hydrothermal synthesis of tin(IV) selenides and the structures of three of them have been determined by single crystal X-ray diffraction. Two of these phases, the orthorhombic and the monoclinic microporous layered forms of $TMA_2Sn_3Se_7$ are polymorphic with their space group highly dependent on the nature and concentration of guest molecules. The third phase, a novel open-framework with formula $TMA_2Sn_5Se_{10}O$ has a zinc blende-type structure with oxygen centered adamantane-type $Sn_4Se_{10}O$ clusters linked together by μ_4-$SnSe_4$ pseudo-tetrahedral tin selenide units. It is discovered that the evolution of products in the hydrothermal synthesis of microporous tin(IV) selenide materials behaves much like the zeolites, in that they both follow Oswald's law of successive reactions. This may be the first time that Oswald's rule has been found to apply to non-oxide open-framework materials. An *in situ* variable temperature PXRD study of the orthorhombic $TMA_2Sn_3Se_7$ material established that the material is stable under nitrogen up to and around 250 °C and under vacuum to *ca.* 300 °C at which temperature the framework collapses.

The similarities observed between the tin(IV) sulfide and selenide systems together with information available from the literature, and the identification of molecular species crystallized during the course of the reaction, have made it possible to propose a model for the formation of porous tin selenide phases based on a modular assembly pathway.

Acknowledgments

G.A.O. thanks the Canada Council for the award of Issac Walton Killam Foundation Fellowship for the period 1995–97. The generous financial assistance of the Natural Sciences and Engineering Research Council of Canada (NSERC), Universal Oil Products (UOP), and the Canadian Space Agency (CSA) in support of this work is deeply appreciated. Invaluable technical assistance from Dr David Young is deeply appreciated.

References

1 A. R. West, *Solid State Chemistry and Its Applications*, John Wiley & Sons Ltd., New York, 1989.
2 B. K. Vainshtein, V. M. Fridkin and V. L. Indenbom, *Structure of Crystals*, Springer-Verlag, New York, 1988.
3 A. R. Verma and P. Krishna, *Polymorphism and Polytypism in Crystals*, John Wiley & Sons, Inc., New York, 1966.
4 W. Oswald, *Z. Phys. Chem.*, 1897, **22**, 289.
5 M. E. Davis and R. F. Lobo, *Chem. Mater.*, 1992, **4**, 756.
6 D. Turnbull, *Phase Changes*, in *Solid State Physics*, ed. F. Seitz and D. Turnbull, Academic Press, New York, 1956.
7 L. S. Ramsdell, *Am. Mineral.*, 1945, **30**, 519.
8 D. W. Breck, *Zeolites Molecular Sieves*, *Structure*, *Chemistry and Use*, John Wiley and Sons, New York, 1974.
9 R. F. Adamsky and K. M. Merz, *Z. Kristallogr.*, 1959, **111**, 350.
10 G. Honjo, S. Miyake and T. Tomita, *Acta Crystallogr.*, 1950, **3**, 396.
11 B. Palosz, W. Palosz and S. Gierlotka, *Acta Crystallogr.*, *Sect. C*, 1985, **41**, 807.
12 B. Palosz, W. Palosz and S. Gierlotka, *Acta Crystallogr.*, *Sect. C*, 1985, **41**, 1402.
13 B. Palosz, W. Palosz and S. Gierlotka, *Acta Crystallogr.*, *Sect. C*, 1986, **42**, 653.
14 A. R. Verma, *Proc. R. Soc. London*, *Ser. A*, 1952, **65**, 525.
15 R. S. Mitchel, *Z. Kristallogr.*, 1957, **109**, 1.
16 A. R. Verma and P. Krishna, *Proc. R. Soc. London*, *Ser. A*, 1957, **240**, 462.
17 B. Palosz, *Phys. Status Solidi A*, 1983, **80**, 11 and references therein.
18 B. Palosz and S. Gierlotka, *Acta Crystallogr.*, *Sect. C*, 1985, 1404.
19 D. I. Bletskan, I. M. Mitrovtsii, V. A. Stefanovich, M. V. Portorii, Yu. V. Voroshilov and V. Yu. Slivka, *Sov. Phys. Crystallogr.*, 1987, **32**, 224.
20 C. L. Bowes, *Ph.D Thesis*, University of Toronto, 1996.
21 T. Jiang, *Ph.D Thesis*, University of Toronto, 1997.
22 T. Jiang, A. L. Lough, G. A. Ozin, D. Young and B. L. Bedard, *Chem. Mater.*, 1995, **2**, 245.
23 G. A. Ozin, *Supramol. Chem.*, 1995, **6**, 125.
24 H. Ahari, Ö. Dag, S. Petrov, G. A. Ozin and R. L. Bedard, *J. Phys. Chem.*, 1998, **102**, 2356.
25 *Cerius2 Simulation Tools User's Reference*, BIOSYM/Molecular Simulations, 1995, p. 195.
26 H. Ahari, R. L. Bedard, C. Bowes, N. Coombs, Ö. Dag, T. Jiang, G. A. Ozin, S. Petrov, A. Verma, G. Vovk and D. Young, *Nature*, 1997, **388**, 857.
27 C. L. Bowes, S. Petrov, G. Vovk, D. Young and G. A. Ozin, *J. Mater. Chem.*, 1998, **8**, 711.
28 W. S. Sheldrick and H. G. Braunbeck, *Z. Naturforsch.*, *Teil B*, 1990, **45**, 1643.
29 J. B. Parise, Y. Ko, K. Tan, D. M. Nellis and S. J. Koch, *J. Solid State Chem.*, 1995, **117**, 219.
30 A. Blecher, M. Dräger and B. Mathiasch, *Z. Naturforsch.*, *Teil B*, 1981, **86**, 1361.
31 O. M. Yaghi, Z. Sun, D. A. Richardson and T. L. Groy, *J. Am. Chem. Soc.*, 1994, **116**, 807.
32 O. M. Yaghi, D. A. Richardson, C. E. Davis, G. Li and T. L. Groy, *Mater. Res. Symp. Proc.*, 1995, **371**, 15.
33 M. Ribes, J. Oliver-Fourcade, E. Philippot and M. Maurin, *J. Solid State Chem.*, 1973, **8**, 195.
34 H. Ahari and G. A. Ozin, 1997, unpublished results.
35 B. Krebs and S. Pohl, *Z. Naturforsch.*, *Teil B*, 1971, **26**, 853.
36 B. Krebs and S. Pohl, *Z. Anorg. Allg. Chem.*, 1976, **424**, 265.
37 B. Krebs and W. Schiwy, *Angew. Chem.*, *Int. Ed. Engl.*, 1975, **14**, 261.
38 B. Krebs, *Angew. Chem.*, *Int. Ed. Engl.*, 1983, **22**, 113.
39 W. M. Meier and D. H. Olson, *Atlas of Zeolite Structure Types*, Butterworth-Heinemann, London, 3rd revised edn., 1992.
40 M. L. Connolly, *J. Appl. Crystallogr.*, 1983, **16**, 548.
41 M. L. Connolly, *Science*, 1983, **221**, 709.
42 T. Jiang, G. A. Ozin and R. L. Bedard, *Adv. Mater.*, 1995, **7**, 166.
43 T. Jiang, G. A. Ozin and R. L. Bedard, *Adv. Mater.*, 1994, **6**, 860.
44 B. Krebs, *Angew. Chem.*, *Int. Ed. Engl.*, 1983, **22**, 113 and references therein.
45 B. Krebs and H.-U. Hürter, *Z. Anorg. Allg. Chem.*, 1980, **462**, 143.
46 W. S. Sheldrick and B. Schaaf, *Z. Anorg. Allg. Chem.*, 1994, **620**, 1041.
47 W. S. Sheldrick and H. G. Braunbeck, *Z. Naturforsch.*, *Teil B*, 1989, **44**, 851.
48 B. Krebs and S. Pohl, *Z. Anorg. Allg. Chem.*, 1972, **241**, 393.
49 D. Young and G. A. Ozin, 1995, unpublished results.
50 Ö. Yükseker, A. L. Lough and G. A. Ozin, 1997, unpublished results.
51 I. D. Gay, C. H. W. Jones and R. D. Sharma, *J. Magn. Reson.*, 1989, **84**, 501.

Paper 8/07660J